LBL--14414

DE83 003051

LBL-14414
CONF-821011--17

DESIGN CONSIDERATIONS FOR A HIGH-SPATIAL-RESOLUTION POSITRON CAMERA WITH DENSE-DRIFT-SPACE MWPC'S *

A. Del Guerra, V. Perez-Mendez, G. Schwartz

Lawrence Berkeley Laboratory
University of California
Berkeley, California 94720

and

W. R. Nelson

Stanford Linear Accelerator Center
Stanford, California 94305

October 1982

* This work was supported by the Director, Office of Energy Research, Office of High Energy and Nuclear Physics, Division of High Energy Physics of the U. S. Department of Energy under Contract No. DE-AC03-76SF00098.

Design Considerations for a High Spatial Resolution Positron Camera with Dense Drift Space MWPC's

A. Del Guerra (*), V. Perez-Mendez, G. Schwartz
Lawrence Berkeley Laboratory, Berkeley, California 94720
and
W.R. Nelson
Stanford Linear Accelerator Center, Stanford, California 94305

Abstract

A multiplane Positron Camera is proposed, made of six MWPC modules arranged to form the lateral surface of a hexagonal prism. Each module (50x50 cm^2) has a 2 cm thick lead-glass tube converter on both sides of a MWPC pressurized to 2 atm. Experimental measurements are presented to show how to reduce the parallax error by determining in which of the two converter layers the photon has interacted. The results of a detailed Monte Carlo calculation for the efficiency of this type of converter are shown to be in excellent agreement with the experimental measurements. The expected performance of the Positron Camera is presented: a true coincidence rate of 56000 counts/s (with an equal accidental coincidence rate and a 30% Compton scatter contamination) and a spatial resolution better than 5.0 mm (FWHM) for a 400 μCi point-like source embedded in a 10 cm radius water phantom.

1. Introduction

As originally proposed[1], the Positron Camera consists of six large area MWPC modules arranged to form the lateral surface of a hexagonal prism. Each 50x50 cm^2 module has a MWPC (45x45 cm^2 active area) sandwiched by two lead-glass tube converters, 2 cm thick each (fig 1). Experimental results obtained with a 15x15 cm^2 test module have already been reported[1,2], as have been preliminary results from the Monte Carlo study of the spatial resolution capability of such a camera[3].

In this paper it is further shown how one can reduce the parallax error by knowing in which of the two converters (top or bottom) the interaction took place. We also discuss the results of the Monte Carlo simulation of the photon interaction within the lead-glass tube converter and we compare the calculated efficiency with experimental data.

Finally, the general performance of the Positron Camera is described and expected count rates are given for β^+ sources in air and in water phantoms.

2. Experimental Results

The 15x15 cm^2 test module chamber has been described elsewhere[1,2]. Briefly, the cathode-cathode gap is 1.0 cm; the anode plane is made of 20 μm wires (3 mm pitch); the cathode planes, consisting of 100μm wires (2 mm pitch), are arranged at 90° relative to each other to allow both x and y localization. The position read-out is done by means of fast delay lines (8ns/cm), capacitively coupled to the cathode plane[4]. Converters with thicknesses up to 4 cm may be accomodated underneath the bottom cathode. The entire assembly is fully contained within a sealed aluminum box which may be pressurized to 2 atm.

2.1 - Efficiency

The converter is made of glass capillaries of high lead content, fused to form honeycomb matrices. The glass matrix is leached in a hydrogen atmosphere to produce a resistive layer, which allows for creation of a uniform voltage gradient. A voltage is applied between the ends of the tubes and the conversion electrons from the 511 keV γ-rays are drifted along the electric field lines and out into the wire avalanche region. The details of the converter construction and treatment processes have been given elsewhere[5]. Various converters of different diameters have been used[6]. Our highest efficiency so far has been obtained with tubes with inner diameters of 0.91 mm and wall thickness of 0.096 mm (80% PbO by weight, density 6.2 g/cm^3). Detection efficiencies for 511 keV γ-rays incident at 90° ± 3.5° onto this type of converter (1 cm thick) are presented in Figure 2 as a function of the discriminator threshold, fed by the anode signal amplified 220 times. Measurements have been made with P_{30} (Argon 70%/Methane 30%) at various pressures with an effective voltage setting (V_{eff}=V_{anode}-$V_{cathode}$) that produces a negligible background count rate. Very stable operation conditions and full reproducibility of the results have been observed over a period of several months. At 2 atm an efficiency of 4.5% has been measured with a plateau longer than 30 dB. At this pressure very large amplitude (up to 40 mV into 50 Ω) and partially saturated pulses were detected with the chamber working close to the self-quenching streamer regime[7]. A spatial resolution of 1.3 mm (FWHM) and a time resolution of 130 ns (FWHM) have been measured with a 1 cm thick converter[2]. The time resolution can be improved by 30% by adding CF_4 gas[6].

2.2 - Top/Bottom Converter Discrimination

Due to the large solid angle subtended by two opposite modules the parallax error may be fairly large for the proposed camera. Annihilation gamma rays which traverse the module at an angle as steep as 30°(see fig. 1) may produce a maximum parallax error of $t_{eff} \times \tan(30°)$, where t_{eff} is the interaction uncertainty along the module depth. If no electronic discrimination is provided, t_{eff} would correspond to the total thickness of the module (i.e. ~6 cm).

Borkowski and Kopp[8] suggested a method for half-gap discrimination in MWPC's used in X-ray imaging by looking at the differences in amplitude and shape of the induced signals on the two cathodes. It has been shown that such a difference depends on the fact that the avalanche is localized on one side of the anode wire[9-12]. With counters operating in the proportional region, however, a characteristic time of several microseconds is required in order to permit clear separation[11]. It has been suggested that if the counter is working in the semi-proportional region[10] or, better yet, in the self-quenching streamer regime[13], this discrimination is more effective, because space charge effects push the center of gravity of the avalanche further away from the anode wire and the top/bottom asymmetry is enhanced.

In the following section we present some experimental measurements that show that discrimination is obtained in less than 50 ns in the self-quenching streamer regime. This enables us to discriminate between the top and bottom converters under the high count rate needed for the Positron Camera.

(*) On Leave from: Istituto di Fisica, Piazza Torricelli 2, Pisa, Italy.

2.2.1 - Measurements with ^{55}Fe and ^{90}Sr Sources

The measurements have been performed with the 15x15 cm^2 test module chamber. To ensure that the counter was working in a self-quenching streamer regime[7], a different anode plane was used (75 μm wires, 4 mm pitch) with a 2 cm cathode-cathode gap (2 atm P_{30} gas).

A schematic drawing of the measurement set-up is shown in fig. 3. The induced signals on the two cathodes were collected by means of copper strips, which simulate the delay lines, placed perpendicular to the cathode wires. A thin mylar foil was interspaced between each copper strip and the corresponding cathode plane. The signal was read onto a load resistor (R_L=1 to 100k Ω) and fed into a Tektronix 475 oscilloscope (see fig. 4). For a ^{55}Fe source (5.9 keV X-ray) it is expected that most of the detected photons interact in the top part of the chamber. The corresponding induced signals are shown in fig. 4a. The overall top/bottom asymmetry is clearly visible with signals of ~50 ns rise time. Fig. 4b shows a similar picture when a ^{90}Sr source (endpoint of the β^- spectrum = 0.546 MeV) is used. The number of avalanches initiated in the top and bottom half-gaps is expected to be much the same, and this is qualitatively confirmed by the figure. Figure 5 shows the corresponding pulse height distribution for the ^{55}Fe source. In this case a 1 k Ω load resistor was used and the two signals were fed through a high input impedance amplifier. The two peaks correspond to avalanches being produced in the two separate half-gaps, which induce bigger pulses on the nearest cathode. As is clearly seen from the figure, most of the interactions occur in the top half-gap (the higher pulse height peak in fig. 5a) and these events correspondingly produce smaller amplitude pulses on the bottom cathode (first peak in fig. 5b) (note that the two figures have a different vertical scale).

In the actual Positron Camera situation, electromagnetic delay line read-out will be used for x and y localization. In order to discriminate between top and bottom converter, it is necessary to also have a prompt signal which can be picked-up from the relative ground of the delay line. A schematic drawing of the experimental set-up is shown in fig. 6. The characteristic impedance (Z_0) of the test delay lines is ~150Ω. The load resistor must be small enough so as not to excessively decrease the amplitude of the slow signal necessary for the position determination. A value of 50Ω was chosen. Differential Amplifiers are used both for position information (DA 1 through 4) and for the analysis of the prompt signal (DA 5). In the arrangement of fig. 6, DA 5 will give a positive output if the top cathode signal is greater than that from the bottom cathode, and a negative signal in the opposite case. The results that we have obtained with a ^{55}Fe source are presented in fig. 7. Integration of the area subtended by the curve shows that 89% of the detected events have a top cathode signal greater than the bottom. That is, 89% of the time the 5.9 keV photon interacts in the top half-gap, which is in good agreement with the calculated value of 85% obtained using the cross sections by Hubble[14].

2.2.2 - Measurements with the β^+ Source

With the same arrangement (see fig. 6) we measured the top/bottom difference with an electronically collimated[1,2] ^{68}Ge source. A 1 cm thick converter was placed underneath the bottom cathode. The converter was set at the appropriate voltage in order to drift the electrons out of the converter and into the avalanche region of the chamber. When no voltage is applied to the converter, the detection of 511 keV γ-rays derives from the interaction of the photon with the inner surface of the aluminum box and with the surface of the converter itself. The results obtained are shown in Table 1. The last column shows the net contribution of the converter, once the surface effects have been subtracted.

In the actual Positron Camera situation we expect to be able to tell whether the interaction occurred in the top or bottom converter with a confidence level of at least 90%, and this reduces the parallax error by almost a factor of three (i.e., thickness of the module/thickness of single converter).

3. Monte Carlo Results

A general electromagnetic radiation transport Monte Carlo code EGS[15] has been used in order to calculate the spatial resolution of the proposed Positron Camera and to determine the contamination due to Coepton scattering in the phantom. A detailed description of how EGS was implemented (i.e., geometry, scoring, etc.) has been given elsewhere[3] and will not be repeated here. Suffice it to say that the real geometry for each lead-glass tube converter, because of the complexity introduced by the very large matrix of cylinders, was approximated by a solid converter whose density was reduced by an appropriate area ratio. Following an interaction in this pseudo-converter, it remains to be decided whether the Compton- or photo-electron will reach a hole and get detected. In a previous paper[3] we assumed, based on range-energy table arguments, that the event was detected if the kinetic energy exceeded 200 keV. A better method of determining this "intrinsic converter efficiency", based on sampling techniques, is described in the next section.

3.1 Intrinsic Detection Efficiency of the Converter

In order to determine the probability that an electron of a given kinetic energy will actually get transported into one of the holes of the converter, we have used the EGS code with a special geometry that corresponds to a "unit cell" (see inset to Fig. 8). Three combinations of inner and outer

Table 1
Top-Bottom Cathode Discrimination for 511 keV γ-rays

	Converter voltage ON	Converter voltage OFF	Net contribution due to the Converter
Absolute Efficiency	4.6×10^{-2}	0.5×10^{-2}	4.1×10^{-2}
Relative contribution			
Bottom > Top	88%	61%	91%
Top > Bottom	10%	11%	9%
|Bottom-Top| < Noise	2%	28%	-

diameters were chosen with the length of the cell fixed at 1 cm and $\rho = 6.2$ g/cm^3.

To simulate the experimental conditions, photons randomly irradiated the top face of the cell at an angle of $90° \pm 3.5°$, and all particles either were transported inside the cell until they reached a cutoff (10 keV or 1 keV for γ or e^-, respectively), exited the top or bottom, or exited the sides. In the latter case, in order to fully realize the actual converter with a multitude of contiguous holes, the particles were re-transported back into the unit cell by making the appropriate coordinate translation while maintaining the direction of motion. When an electron entered the inner diameter of the cell, it was considered to be detected irrespective of its energy at that point.

The probability for an electron to reach a hole depends on its energy, where it is created, and its direction of motion. By throwing photons over the unit cell and scoring the energy release into two histograms (detected events and total events), we are able to determine the probability that an electron with a given kinetic energy will reach a hole —— averaged over the various positions and directions.

Fig. 8 shows the average detection probability as a function of energy for three different tube sizes. Tubes with inner/outer diameter of 1.33 mm/1.59 mm and 0.91 mm/1.10 mm, respectively, have already been used for converter prototypes[5,6]. The upper curve refers to a new type of converter with inner and outer diameter tubing of 0.48/0.60 mm, which is now being tested. A photon of 511 keV produces a photoelectron in the lead-glass with a kinetic energy of 425 keV. For the 0.91 mm/1.10 mm tube this interaction has (on the average) a probability of ~1/3 to be detected. Hence, the efficiency of such a converter of any thickness for 511 keV photons must always be less than ~33%. Fig. 8 shows that smaller diameter tubes (i.e. 0.48mm/0.60mm) will increase this limit to ~50%.

The calculated efficiencies for these three types of converters are presented in fig. 9 as a function of the photon energy and are compared with experimental data at 511 keV, where excellent agreement is seen. Fig. 9 also shows that the efficiency of a dense drift space MWPC diminishes with decreasing energy of the incident photon; this behavior is opposite to that of a crystal-type detector.

The dotted curve in fig. 9 shows the calculated efficiency for one module of the proposed Positron Camera. In this case there are two layers of converter, 2 cm thick each, with tubes of 0.91mm/1.10 mm. A correction to account for the increase in converter thickness, due to the angle of incidence ($\pm 30°$) (see fig. 1), has been included. An efficiency of 15% is expected for 511 keV γ-rays; if the tube diameters were 0.48mm and 0.60 mm the efficiency would be a factor 1.5 higher.

3.2 - Spatial Resolution and Compton Scatter Contamination

The EGS code has also been used to study both the spatial resolution and the Compton scatter contamination in the presence of water phantoms. As stated previously, a pseudo-converter of reduced density was employed and the probability of detection, based on curves provided in the previous section, was included by means of sampling.

Several factors contribute to the spatial resolution of the system: positron range, two-gamma non-collinearity, Compton scattering in the phantom, and intrinsic detector resolution. With our Monte Carlo simulation it has been possible to study the absolute contribution of each to the overall spatial resolution. Table 2 shows the results, which have been obtained for a 10 cm radius water phantom and a ^{11}C point-like source at its center.

Table 2
Contribution to the Positron Camera Spatial Resolution for a ^{11}C Source

	FWHM(mm)
Positron range	0.4
Two gamma non-collinearity	2.2
Detector response:	
- Parallax error	2.4
- Intrinsic spatial resolution	2.4
Overall spatial resolution	5.5

As already mentioned in the previous section, the efficiency of the dense drift space MWPC diminishes with decreasing photon energy, and it is almost zero for photon energies less than 100 keV (i.e. fig. 9). For such a reason, Compton scattering is much less important here than for scintillation cameras. Its net effect for a 10 cm radius water phantom is to reduce both the single and coincidence rate by a factor 1.5 and 3, respectively.

Furthermore, approximately one third of the coincidence events are found to be uniformly distributed within the phantom, whereas the smearing of the spatial resolution is negligible (<0.1 mm FWHM).

In table 3 the calculated spatial resolution (FWHM) is presented for various positron emitters together with some of their physical parameters. The difference in spatial resolution among the various isotopes is almost entirely due to the different contributions of the positron range[3].

4. Performance and Count Rates of the Proposed Positron Camera

The expected performance and count rates of the proposed Positron Camera are summarized in Table 4. The count rates in air have been calculated using the relation [3]

$$\frac{c^2}{2\tau} = \frac{T^2}{A}$$

with the condition T=A, where c is the efficiency of a single module, τ its time resolution, T and A the true and accidental coincidence rate, respectively. The count rates in the presence of a water phantom have been scaled down using the Monte Carlo results.

In conclusion, the tomograph we propose has an intrinsic three-dimensional capability with fields of view of 20-30 cm. A spatial resolution better than

Table 3
Positron Emitters Characteristics and Spatial Resolution

	^{18}F	^{11}C	^{68}Ga	^{82}Rb
Mean Life (m)	109.9	20.38	68.1	1.25
End-point of the β^+ spectrum (MeV)	0.635	0.961	1.899	3.335
Spatial Resolution (FWHM) (mm)	4.8	5.5	6.5	8.2

Table 4
Performance and Count Rates of the Proposed Camera

Positron Camera Module Specifications	
MWPC active area	45 x 45 cm^2
Converter thickness	(2 + 2) cm
Gas pressure	2 atm
Efficiency	15%
Positron Camera Performance	
Coincidence Efficiency	1%
Coincidence Resolving time	200 ns
Spatial Resolution (for ^{18}F) (FWHM)	4.8mm
Count Rates for a 400 μCi point-like source (T/A=1) in Air	
Single Rate per module	375 x 10^3 counts/s
True coincidence rate per module pair	56 x 10^3 counts/s
True coincidence rate for the system	168 x 10^3 counts/s
Count Rates for a Activity of 0.1 μCi/ml (T/A = 1) in a 10 cm Radius, 10 cm long water phantom	
True coincidence rate for the system	56 x 10^3 counts/s
Number of simultaneous slices (1 cm thick)	10
True coincidence rate per slice	5600 counts/s
Number of voxels per slice (0.6x0.6x1.0 cm^3)	870
True coincidence rate per voxel in one minute	400 counts/m
Compton distributed noise	~1/3
Statistical uncertainty of the signal (total-accidental) per voxel in one minute	12%

5.0 ns (FWHM) can be attained. Ten simultaneous slices (1 cm thick) may be obtained with 10^6 true coincidence counts for each slice in 3 minutes and with a total sensitivity of 56000 counts for 0.1 μCi per cm^3 of activity in a 10 cm radius phantom.

References

(1) A. Del Guerra, C.B. Lim, G.K. Lum, D. Ortendahl, and V. Perez-Mendez, "Medical positron imaging with a dense drift space Multi-Wire Proportional Chamber", Lawrence Berkeley Laboratory, LBL-14043 (March 1982), and IEEE Trans. Med. Imag., Vol. TMI-1, 1982, in press.

(2) A. Del Guerra, V. Perez-Mendez, G. Schwartz, and B. Sleaford, "High Spatial Resolution MWPC for Medical Imaging with Positron Emitters", Lawrence Berkeley Laboratory, LBL-14044 (March 1982), and Proceedings of the "Int. Conf. on Applications of Physics of Medicine and Biology", Trieste (Italy), 30 March - 3 April 1982, Ed. by: G. Alberi, Z. Bajzer, and P. Raza, World Scientific Publishing Co., Singapore, 1982, in press.

(3) V. Perez-Mendez, A. Del Guerra, W.R. Nelson, and K.C. Tam, "The Imaging Performance of a MultiWire Proportional Chamber Positron Camera", Lawrence Berkeley Laboratory, LBL-14114, (October 1982), and to be presented at the First IEEE Computer Society International Symposium on Medical Imaging and Image Interpretation, Berlin, West Germany, 26-29 October 1982.

(4) P. Lecomte, V. Perez-Mendez and G. Stuker, "Electromagnetic Delay Lines in Spark, Proportional and Drift Chamber Applications", Nucl. Instr. and Meth., Vol 153, pp. 543-551, 1978.

(5) G.K. Lum, M.I. Green, V. Perez-Mendez and K.C. Tam, "Lead Oxide Glass Tubing Converters for Gamma Detection in MWPC", IEEE Trans. Nucl. Sci., Vol. NS-27, pp. 157-165, 1980.

(6) G.K. Lum, V. Perez-Mendez, and B. Sleaford, "Gamma-Ray Detection with PbO Glass Converters in MWPC: Electron Conversion Efficiency and Time Resolution", IEEE Trans. Nucl. Sci., Vol. NS-28, pp. 821-824, 1981.

(7) T.A. Mulera, A. Del Guerra, V. Perez-Mendez, and G. Schwartz, "Large Signal Production in Wire Chambers Filled with Noble Gas-Carbon Dioxide and Noble-Gas Hydrocarbon Mixtures", Lawrence Berkeley Laboratory, LBL-14412 (October 1982), and to be presented at the 1982 IEEE NS-Symposium, Washington, D.C., October 20-22, 1982; and references therein.

(8) C.J. Borkowski and M.K. Kopp, "Electronic Discrimination of the Effective Thickness of Proportional Counter", IEEE Vol. NS-24, No. 1, pp. 287-292, 1977.

(9) J. Fischer, H. Okuno, and A.H. Walenta, "Avalanche Localization and its effects in proportional counter", IEEE Vol. NS-25, pp. 794-799, 1978.

(10) J. Fischer, H. Okuno, and A.H. Walenta, "Spatial Distribution of the Avalanche in proportional counters", Nucl. Instr. and Meth., Vol. 151, pp. 451-460, 1978.

(11) A.H. Walenta, "Left-Right Assignment in Drift Chambers and MWPC's using Induced Signals", Nucl. Instr. and Meth., Vol. 151, pp 461-472, 1978.

(12) H. Okuno, J. Fischer, V. Radeka, and A.H. Walenta, "Azimuthal spread of the avalanche in proportional chambers", IEEE Vol. NS-26, pp. 160-168, 1979.

(13) G.D. Alekseev, N.A. Kalinina, V.V. Karpukhin, D.M. Khazins, and V.V. Kruglov, "Investigation of self-quenching streamer discharge in a wire chamber", Nucl. Instr. and Meth., Vol. 177, pp. 385-397, 1980.

(14) J.H. Hubbel, "Photon Mass Attenuation and Mass Energy-Absorption Coefficients for H,C,N,O, Ar, and Seven Mixtures from 0.1 keV to 20 MeV", Radiation Research, Vol. 70, pp. 55-81, 1977.

(15) R.L. Ford and W.R. Nelson, "The EGS Code system: Computer programs for the Monte Carlo Simulation of Electromagnetic Cascade Showers (Version 3)", Stanford Linear Accelerator Center, SLAC-210, June 1978.

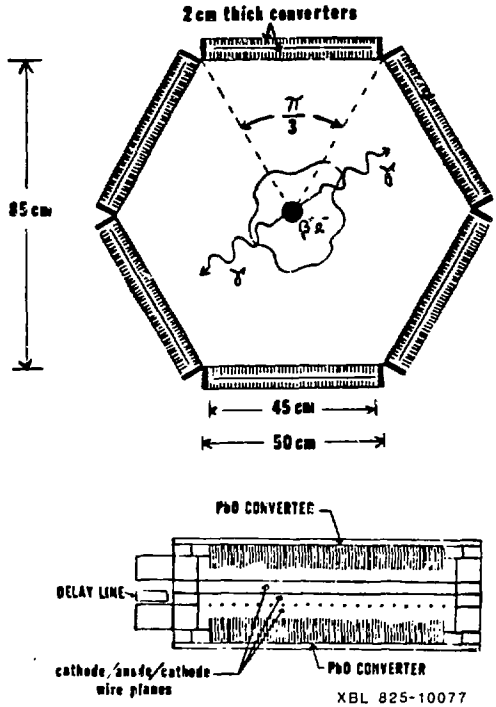

Fig. 1 The proposed Positron Camera, made of six modules arranged to form a hexagonal prism: plan view of the camera (TOP); cross view of a single module (BOTTOM).

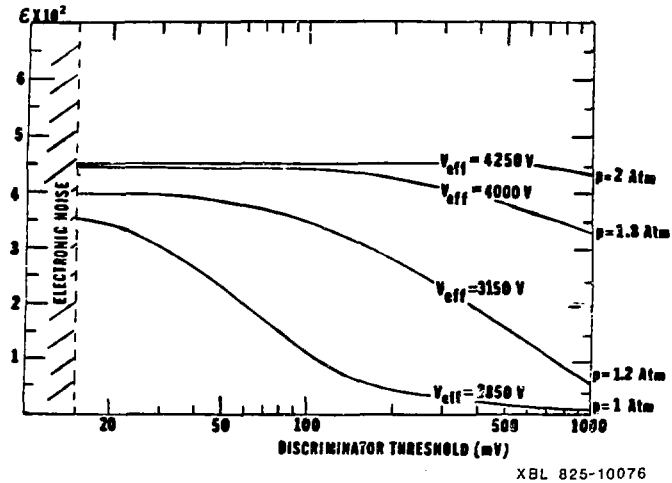

Fig. 2 Efficiency of the 15x15 cm^2 module as a function of anode discriminator threshold at various pressures.

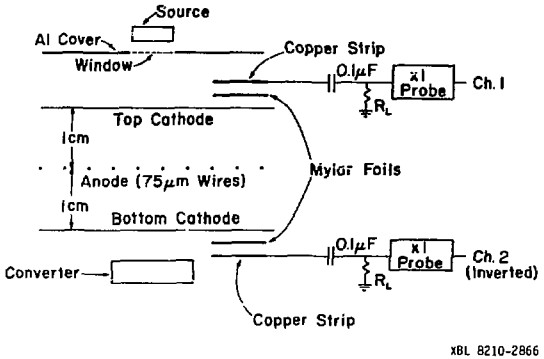

Fig. 3 Schematic drawing of the experimental set-up to measure top/bottom cathode asymmetry.

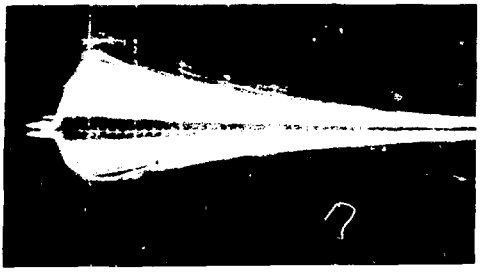

a

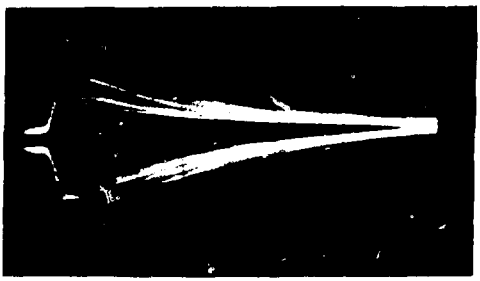

b

Fig. 4 Induced cathode pulses into a 10 kΩ load resistor showing top/bottom asymmetry: (a) ^{55}Fe source, (b) ^{90}Sr source. (Hor. scale 100 ns/div.; vert. scale 50 mv/div.).

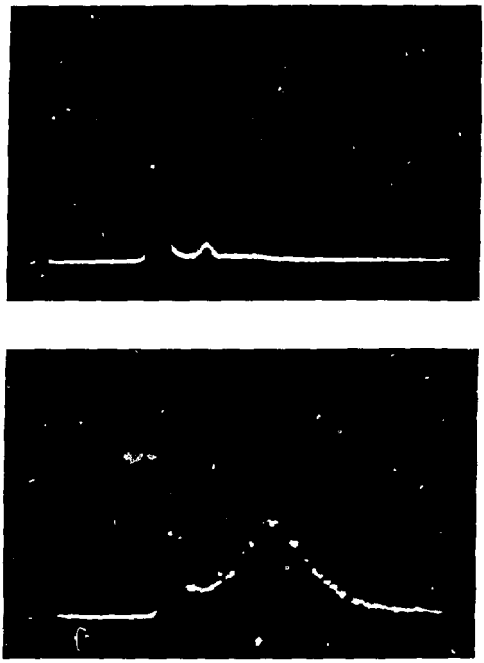

Fig. 5 Typical pulse height spectra of the induced cathode signals for a ^{55}Fe source: top cathode, full vertical scale 512 counts (TOP); bottom cathode, full vertical scale 2k counts (BOTTOM).

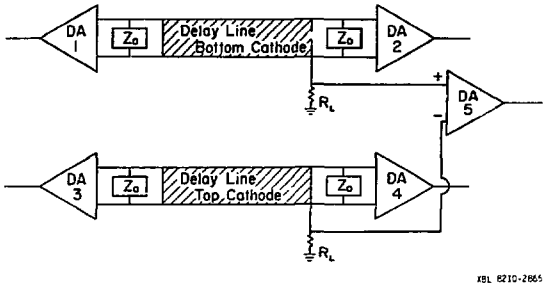

Fig. 6 Schematic drawing of the delay line electronic set-up for both position read-out and top/bottom converter discrimination.

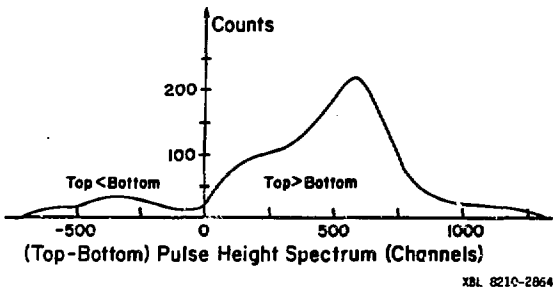

Fig. 7 Pulse height spectrum showing the difference between the top and bottom cathodes. A differential amplifier was used to obtain the spectrum. The bottom > top part of the spectrum has been inverted for the figure.

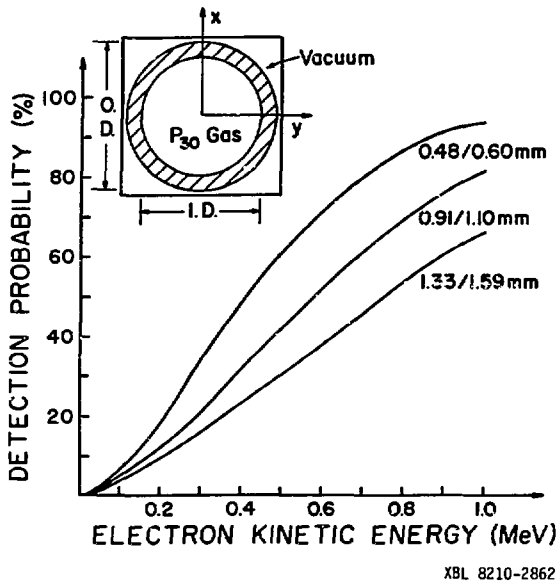

Fig. 8 Calculated electron detection probability as a function of its kinetic energy for three different (I.D./O.D.) converter tubes Inset: unit cell used for the Monte Carlo calculation.

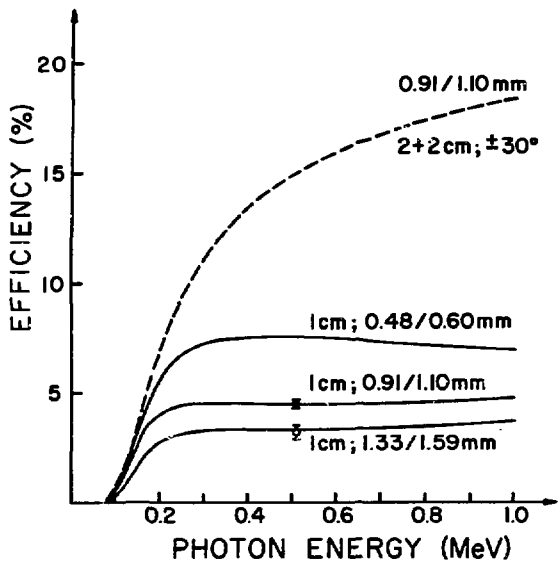

Fig. 9 Calculated efficiency of the converter as a function of the photon energy: 1 cm thick and three different I.D./O.D. converter tubes (solid lines); O-experimental data from ref. 6; ●-this experiment. The dotted line shows the calculated efficiency for one module of the proposed Positron Camera.